GER 12577

COMPUTER STUDY TO DETERMINE THE EFFECT OF BALLOON FOOTPRINT AND OPTICAL CHARACTERISTICS ON MATERIAL TEMPERATURES OF A SPHERE ON THE LUNAR SURFACE FOR HIGH-NOON CONDITION

January 1966

Prepared under Contract NAS 1-5778

by
Goodyear Aerospace Corporation
Akron, Ohio

for

National Aeronautics and Space Administration
Langley Research Center

FOREWORD

This report presents a six-week study for determining the temperature distribution on a spherical lunar landing aid. This program was authorized under contract NAS 1-5778.

Technical direction, problem definition, and physical constants were provided by Mr. William J. O'Sullivan, Assistant-to-the Chief, Applied Materials and Physics Division, Langley Research Center, National Aeronautics and Space Administration.

The Goodyear Aerospace Corporation participants were J. N. Apisa, R. L. Ginter, P. G. Kost, and F. J. Stimler.

SUMMARY

36783

An analysis was made to determine the temperature distribution of a 12-foot balloon, with a diffuse surface, sitting on the lunar surface at high noon (fig. 1) with two different footprints, 30^{o} and 150^{o}. The optical properties of the external surface were varied through several different values. Both the solar absorptance and total emittance have an appreciable effect on the temperatures. The smaller the footprint the smaller the range of the average temperature for the various emittances.

The lunar properties of emittance and absorptance were varied through a range that would cover most published values for maximum lunar surface temperatures, 250 to 270^{o}F. The effects on the balloon temperatures were minor.

In general, the use of a rigidized sphere for a lunar landing aid appears very feasible since the footprint is not critical from a thermal standpoint, internal pressurization is not required, and a reflective sphere with a thin coating, which increases the emittance, results in very favorable temperatures for the Mylar.

Author

CONTENTS

ILLUSTRATIONS

TABLES

INTRODUCTION

The 12-foot diameter sphere being analyzed in this report is an item that could be packaged into a small envelope on a spacecraft and later deployed. The sphere must not only be packageable and deployable, but also must be able to survive the environment of outer space, such as ultraviolet radiation, solar wind, thermal radiation, and micrometeoroids.

Goodyear Aerospace has worked in the area of inflatable structures for several years and has developed techniques and capabilities along these lines. The basic structure being considered here was a grid spherical structure that can be stretch-formed by a thin-walled balloon, thus causing it to be unaffected by micrometeoroid punctures, since it does not require that any internal pressure be maintained. The thin envelope in this case is a necessary component and must be supported and remain intact. GAC has fabricated structures of this type and investigated related thermal problem areas. Some of the deployable items have been solar energy concentrators, grid spheres, pseudo-passive satellites, Manned Orbiting Laboratory tunnels, space garages, and Stay Time Extension modules (STEM). All of these units have required thermal control coatings that could be applied to a nonrigid substrate such as Mylar. GAC has investigated two types of cold coatings having low ratios of solar absorptance to total emittance - a white silicone paint and SiO on aluminized film. Lightweight coatings, a few microns of silicone paint on several hundred angstroms of vacuum-deposited aluminum, were investigated for solar concentrators where materials behind the mirrored surface required that temperatures be held below some maximum.

Most of these investigations required development of an analytical thermal model including all modes of heat transfer and all types of heating. Transient analyses of orbiting vehicles include solar heating, both directly and planet reflected (albedo), and infrared heating (planet emitted). GAC developed programs for solution of models on digital computers.

The STEM program involved a cylinder with hemispherical ends sitting on the lunar surface. For a non-moving structure and the long lunar days, these problems are of the steady-state heat balance type. The STEM program and the balloon being analyzed here are both of this type.

Here, a thin-skinned balloon is deployed on the lunar surface. Due to its own weight and structural rigidity, the sphere will flatten to some degree on the bottom; without the presence of any other forces, and if the material does not lose rigidity due to high temperatures, it should remain in a shape similar to that shown in figure 1. The sun is directly overhead. Some of the solar reflections from the balloon are incident on the nearby lunar surface, and some of the solar reflections from the lunar surface strike the balloon. The balloon and the nearby lunar surface exchange infrared emission and come to the same equilibrium temperature. The balloon overhang causes a cool, shaded lunar surface next to the balloon, while immediately outside of this zone is an area of the lunar surface getting extra heat from the reflecting sphere. This area will have a temperature somewhat higher than the lunar surface that is further from the balloon. Determination of these lunar temperature profiles is one of the goals of this analysis; the main objective is the determination of the temperature profile around the balloon.

Table I lists the relevant thermal properties of the cases to be examined.

TABLE I. - CASES EXAMINED

Properties	Case number									
	1	2	3	4	5	6	7	8	9	10
Footprint angle, degrees	150	150	150	150	150	150	150	150	30	30
Balloon solar absorptance	0.10	0.15	0.20	0.10	0.15	0.20	0.15	0.15	0.15	0.15
Balloon external emittance	0.03	0.03	0.03	0.40	0.40	0.40	0.15	0.28	0.03	0.40
Balloon internal emittance	0.40	0.40	0.40	0.40	0.40	0.40	0.40	0.40	0.40	0.40
Lunar solar absorptance	0.93	0.93	0.93	0.93	0.93	0.93	0.93	0.93	0.93	0.93
Lunar emittance	0.85	0.85	0.85	0.85	0.85	0.85	0.85	0.85	0.85	0.85

SYMBOLS AND DEFINITIONS

$\|B\|$	matrix of internal balloon shape factors	T	temperature
$\|C\|$	matrix of external balloon and moon shape factors	α_B	absorptance of balloon
		α_M	lunar absorptance
F_{i-j}	shape factor from node i to node j	ϵ_{BI}	emittance of inner surface of balloon
Q_i	direct solar and/or albedo heating on node i ($Btu/hr\text{-}ft^2$)	ϵ_{BO}	emittance of outer surface of balloon
		ϵ_M	lunar emittance
S	solar constant (442.6 $Btu/hr\text{-}ft^2$)	σ	Stefan-Boltzmann constant (0.1714×10^{-8} $Btu/hr\text{-}ft^2\text{-}{}^oR^4$)

absorptance (solar absorptance) - the ratio of absorbed solar flux to incident solar flux

albedo - the ratio of reflected solar flux to incident solar flux. This pertains only to the moon in this analysis.

conductance - the reciprocal of resistance. In the network analogy this is usually A_iF_{i-j} or $\frac{A_i \epsilon_i}{1-\epsilon_i}$; $A_i \frac{\text{absorptance (IR)}}{\text{reflectance (IR)}}$.

emittance - the ratio of thermal radiation flux from a body to the thermal radiation flux from a black body at the same temperature

IR - infrared

network analogy - a method of analyzing radiation heat transfer by making electrical analogies of thermal quantities

nodes - finite segments into which an object is broken up for purposes of thermal study

resistance - the ratio of voltage to current in electricity. The thermal analogy is the ratio of σT^4 to heat flow.

view (or shape) factor - the view (or shape) factor from (1) to (2) is the fraction of radiation emitted from (1) that strikes (2).

THEORETICAL ANALYSIS

General

The thermal model was constructed with the balloon and moon surface broken up into nodes (fig. 2). The thermal model basically consists of making thermal balances on each node. That is, for the steady-state condition of this analysis, the heat received minus the heat leaving must equal zero for each node. This becomes fairly intricate, since the following heat terms must be accounted for:

(1) Direct solar heating on balloon and moon

(2) Reflected solar radiation off moon's surface to balloon (albedo heating)

(3) Heat exchange between outer surface of balloon and moon

(4) Heat exchange between inside areas (nodes) of balloon

The first two kinds of heating are heating in the solar spectrum. The last two are infrared. The infrared reflections will be considered as multiple; solar reflections from the moon (albedo) will be included, but solar reflections from the balloon will be neglected. Although neglecting the reflections from the balloon introduces a slight error, the effect of this error is that the moon temperatures would be only slightly higher than given by this analysis. The effect on the balloon temperatures should be negligible.

It was found to be undesirable to set up a general computer program in which the footprint angle could be read in as a variable. Both configuration models could be set up and solved more quickly if they were handled separately, because the determination of external shape factors is very rapid when a graphical method is used. The models for the two configurations are basically similar. Although there are different shape factors and peculiarities for each configuration, the thermal properties of the moon and for each configuration of the balloon can be read in as inputs and require no modification of the program. A general flow chart of the analytical procedures is shown in figure 3.

Assumptions

The following assumptions were made in developing the model:

(1) Steady-state heat transfer.

(2) Radiation is the only mode of heat transfer.

(3) Balloon is thermally thin (i.e., for any point on the balloon, outside temperature is the same as inside temperature).

(4) No direct heat transfer from footprint to moon.

(5) Infrared reflections will be considered to be multiple and diffuse.

(6) Solar constant is 442.6 Btu/hr-ft^2

(7) Sun is directly overhead.

(8) Lunar absorptance is 0.93.

(9) Lunar emittance is 0.85.

(10) Balloon has zero transmittance to both solar and infrared radiation.

(11) Negligible solar reflections except from the moon to the balloon.

A sensitivity analysis was made of several of the variables in order to see their effect. For example, the lunar emittance was bracketed (0.85 ± 0.07), as well as the lunar absorptance (0.93 ± 0.02). The lunar absorptance figure of 0.93 (reflectance of 0.07) seems fairly well fixed in the literature (ref. 1). The emittance figure of 0.85 was calculated, based on a lunar surface temperature of 130°C as specified by the contract. This emittance was calculated by the following heat balance on the surface of the moon.

Heat emitted = heat absorbed

$$\epsilon_M \sigma T^4 = \alpha_M S,$$

where

ϵ_M = lunar emittance ($\alpha_M S/\sigma T^4$)

S = solar constant (442.6 Btu/hr-ft^2)

α_M = lunar absorptance (0.93)

σ = Boltzman's constant (0.1714 x 10^{-8} Btu/hr-ft^2-$^\circ$R^4)

T = temperature ($^\circ$R) (726.3°R, $\approx$ 130°C)

resulting in an ϵ_M of 0.85.

Network Method

The network method is used because it is the most feasible method of handling multiple reflections. If the balloon problem were to be solved without the network method, an infinite series of terms would be necessary to handle infrared reflections from node i to node j, then back from j to i, then from i to j, etc. For example:

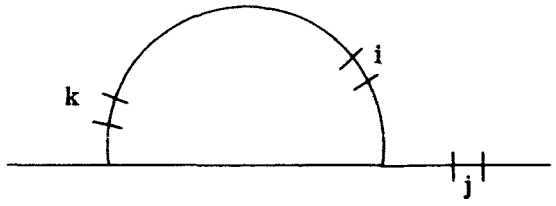

i - node considered
j - node on moon
k - other node on balloon with which i exchanges heat

In making a heat balance on node i, the following heat terms are relevant:

Direct solar + moon albedo + infrared from j + infrared from k = emitted infrared to j and k + net multiple reflection emitted.

$$\alpha_B A_{i(normal)}\, S + A_i\, F_{i-M}\,(1 - \alpha_M)\, S\, \alpha_B + \epsilon_{BO}\, A_{i_j}\, \Sigma F_i - j\, \epsilon j\, \sigma T_j^4 +$$

$$\epsilon_{BI} A_{i_k}\, \Sigma F_{i-k}\, \epsilon_k \sigma T_k^4 = A_i\,(\epsilon_{BI} + \epsilon_{BO})\, \sigma T_i^4 - \beta.$$

β is representative of an infinite series of terms to account for the multiple reflections between i and k, and between i and j. Since this would be impractical to solve, a network method of analysis was used.

This method of analysis was essentially to employ an electrical analogy to the radiation heat transfer problem (ref. 2). In the analogy the heat flow is regarded as current, the quantity (σT^4) is regarded as voltage, and the emittances and shape factors are used as resistances. Each real node has one or two corresponding dummy nodes, depending on whether it exchanges heat on one side (e. g. , node on lunar surface) or on both sides (e. g. , node on balloon). When a real node exchanges heat with its dummy node, the conductance is $A_i(\epsilon_i/1 - \epsilon_i)$. Real nodes only exchange heat with their dummy nodes. Dummy nodes exchange heat with all other dummy nodes they can "see", but only with their corresponding real node. For example, in the following configuration:

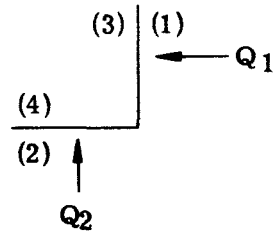

(1) and (2) are real nodes and (3) and (4) are their corresponding dummy nodes.

ϵ_1 is emittance of 1 and ϵ_2 is emittance of 2.

A_1 is the area of 1 and A_2 is the area of 2.

F_{1-2} is shape factor from 1 to 2; F_{2-1} is shape factor from 2 to 1.

Q_1 and Q_2 are direct solar heating on 1 and 2.

Note: $A_1\, F_{1-2} = A_2\, F_{2-1}$.

The conductance between (1) and (3) is $A_1 \frac{\epsilon_1}{1 - \epsilon_1}$

The conductance between (2) and (4) is $A_2 \frac{\epsilon_2}{1 - \epsilon_2}$

The conductance between (3) and (4) is $A_1 F_{1-2}$ or $A_2 F_{2-1}$

This can be shown by the following network:

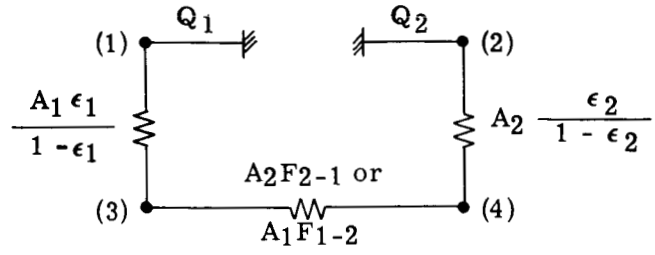

Using the analogy $I = E \frac{1}{R}$ or $Q = (\sigma T^4) \cdot C$,

the net heat on (1) is $A_1 \frac{\epsilon_1}{1 - \epsilon_1} (\sigma T_1^4 - \sigma T_3^4) = Q_1$.

the net heat on (2) is $A_2 \frac{\epsilon_2}{1 - \epsilon_2} (\sigma T_2^4 - \sigma T_4^4) = Q_2$.

the net heat on (3) is $A_1 \frac{\epsilon_1}{1 - \epsilon_1} (\sigma T_3^4 - \sigma T_1^4) + A_1 F_{1-2} (\sigma T_3^4 - \sigma T_4^4) = 0$

the net heat on (4) is $A_2 \frac{\epsilon_2}{1 - \epsilon_2} (\sigma T_4^4 - \sigma T_2^4) + A_2 F_{2-1} (\sigma T_4^4 - \sigma T_3^4) = 0$

After some manipulation, the four heat balances above can be put into the following matrix form:

$$\begin{bmatrix} \frac{\epsilon_1}{1 - \epsilon_1} & 0 & -\frac{\epsilon_1}{1 - \epsilon_1} & 0 \\ 0 & \frac{\epsilon_2}{1 - \epsilon_2} & 0 & -\frac{\epsilon_2}{1 - \epsilon_2} \\ -\frac{\epsilon_1}{1 - \epsilon_1} & 0 & \frac{\epsilon_1}{1 - \epsilon_1} + F_{1-2} & -F_{1-2} \\ 0 & -\frac{\epsilon_2}{1 - \epsilon_2} & -F_{2-1} & \frac{\epsilon_2}{1 - \epsilon_2} + F_{2-1} \end{bmatrix} \begin{bmatrix} \sigma T_1^4 \\ \sigma T_2^4 \\ \sigma T_3^4 \\ \sigma T_4^4 \end{bmatrix} = \begin{bmatrix} Q_1/A_1 \\ Q_2/A_2 \\ 0 \\ 0 \end{bmatrix}$$

This matrix can then be rather easily solved for temperatures. Only the temperatures of the real nodes are of importance.

For the case in point, the procedure is similar to the example. However, there are many more nodes, which complicates the setup of the model and requires more computer running time than the simple model above would require. The shape factor determination can be regarded as a separate problem, and will be discussed later.

A radiation network was set up for each configuration. Heat balances were performed on each node and a matrix was set up. Tables II and III show the matrices that were solved on the computer. The matrices were solved directly for σT_i^4 and indirectly for temperature, T. The extreme right-hand column of the matrices contains Q_i, the direct solar and/or albedo heating term on node i. This is further discussed in the section on direct solar and albedo heating.

TABLE II. - MATRIX FOR 150° FOOTPRINT CASES

$$\epsilon_I = \frac{\epsilon_{BI}}{1 - \epsilon_{BO}} \qquad \epsilon_{M'} = \frac{\epsilon_M}{1 - \epsilon_M}$$

$$\epsilon_O = \frac{\epsilon_{BO}}{1 - \epsilon_{BO}} \qquad \epsilon_{IO} = \epsilon_I + \epsilon_O$$

[|B| and |C| are defined in tables IV and VI.]

	1	. . . .	13	14	15	16	17	18	. . . .	30	31	32	33	. . . .	45	46	47	48		49
1	ϵ_{IO}							$-\epsilon_I$					$-\epsilon_O$						σT_1^4	Q_1
.	ϵ_{IO}							$-\epsilon_I$					$-\epsilon_O$							
.		ϵ_{IO}							$-\epsilon_I$					$-\epsilon_O$						
.			ϵ_{IO}							$-\epsilon_I$					$-\epsilon_O$					
.				ϵ_{IO}							$-\epsilon_I$					$-\epsilon_O$				
13					ϵ_{IO}							$-\epsilon_I$					$-\epsilon_O$			
14						ϵ_I							$-\epsilon_I$							
15							ϵ_I							$-\epsilon_I$						
16							$\epsilon_{M'}$										$-\epsilon_{M'}$			
17							$\epsilon_{M'}$											$-\epsilon_{M'}$		Q_{17}
18	$-\epsilon_I$							$1+\epsilon_I$	- |B| added to this block.											
.		$-\epsilon_I$							$1+\epsilon_I$											
.			$-\epsilon_I$							$1+\epsilon_I$										
.				$-\epsilon_I$							$1+\epsilon_I$									
.					$-\epsilon_I$							$1+\epsilon_I$								
30						$-\epsilon_I$							$1+\epsilon_I$							
31							$-\epsilon_I$							$1+\epsilon_I$						
32							$-\epsilon_I$											$1+\epsilon_I$		
33	$-\epsilon_O$												$1+\epsilon_O$	- |C| added to this block.						
.		$-\epsilon_O$												$1+\epsilon_O$						
.			$-\epsilon_O$												$1+\epsilon_O$					
.				$-\epsilon_O$												$1+\epsilon_O$				
.					$-\epsilon_O$												$1+\epsilon_O$				
45						$-\epsilon_O$												$1+\epsilon_O$		
46							$-\epsilon_{M'}$												$1+\epsilon_{M'}$	
47							$-\epsilon_{M'}$												$1+\epsilon_{M'}$	
48																			ϵ_M	σT_{48}^4 $\alpha_M S$

TABLE III. - MATRIX FOR 30° FOOTPRINT CASES

$$\epsilon_I = \frac{\epsilon_{BI}}{1 - \epsilon_{BO}} \qquad \epsilon_{M'} = \frac{\epsilon_M}{1 - \epsilon_M}$$

$$\epsilon_O = \frac{\epsilon_{BO}}{1 - \epsilon_{BO}} \qquad \epsilon_{IO} = \epsilon_I + \epsilon_O$$

[|B| and |C| are defined in tables V and VII.]

	1	.	.	.	.	11	12	13	14	15	16	17	.	.	.	.	27	28	29	.	.	.	.	39	40	41	42	43	44	45
1	ϵ_{IO}											$-\epsilon_I$							$-\epsilon_O$											σT_1^4	Q_1
.		ϵ_{IO}											$-\epsilon_I$							$-\epsilon_O$											
.			ϵ_{IO}											$-\epsilon_I$							$-\epsilon_O$											
.				ϵ_{IO}											$-\epsilon_I$						$-\epsilon_O$											
.					ϵ_{IO}											$-\epsilon_I$					$-\epsilon_O$											
11						ϵ_{IO}											$-\epsilon_I$					$-\epsilon_O$										
12							ϵ_I										$-\epsilon_I$					$-\epsilon_O$										
13								$\epsilon_{M'}$															$-\epsilon_{M'}$								
14									$\epsilon_{M'}$															$-\epsilon_{M'}$							
15										$\epsilon_{M'}$															$-\epsilon_{M'}$						
16											$\epsilon_{M'}$																$-\epsilon_{M'}$				Q_{16}
17	$-\epsilon_I$											$1+\epsilon_I$																			
.		$-\epsilon_I$											$1+\epsilon_I$																		
.			$-\epsilon_I$											$1+\epsilon_I$																	
.				$-\epsilon_I$											$1+\epsilon_I$																
.					$-\epsilon_I$											$1+\epsilon_I$															
27						$-\epsilon_I$											$1+\epsilon_I$														
28							$-\epsilon_I$											$1+\epsilon_I$													
29	$-\epsilon_O$																		$1+\epsilon_O$											
.		$-\epsilon_O$																	$1+\epsilon_O$											
.			$-\epsilon_O$																	$1+\epsilon_O$										
.				$-\epsilon_O$																	$1+\epsilon_O$										
.					$-\epsilon_O$																	$1+\epsilon_O$									
39						$-\epsilon_O$																	$1+\epsilon_O$								
40								$-\epsilon_{M'}$															$1+\epsilon_{M'}$								
41									$-\epsilon_{M'}$															$1+\epsilon_{M'}$							
42										$-\epsilon_{M'}$															$1+\epsilon_{M'}$						
43											$-\epsilon_{M'}$																$1+\epsilon_{M'}$				
44																													ϵ_M	σT_{44}^4	α_{MS}

$-|B|$ added to this block.

$-|C|$ added to this block.

Shape Factors

The determination of shape factors involved two problems: (1) internal shape factors and (2) external shape factors.

Internal shape factors. - The internal shape factors were determined in the following fashion:

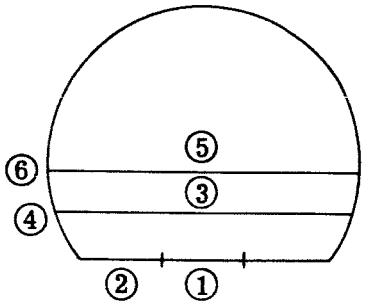

Note: The numbering of the nodes in this sketch does not correspond to actual node numbers.

Shape factors are only needed between all the real nodes. The shape factor between two discs is:

$$F_{a-b} = 0.5\left[\frac{h^2+1}{r^2} + 1 - \sqrt{\left(\frac{h^2+1}{r^2}+1\right)^2 - \frac{4}{r^2}}\right],$$

where

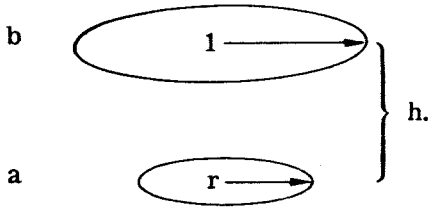

This allows computation of F_{1-3} and $F_{(1+2)-3}$.

Then:

$$F_{1-4} = 1 - F_{1-3}$$

$$F_{(1+2)-4} = 1 - F_{(1+2)-3}$$

$$F_{4-1} = \frac{A_1}{A_4} F_{1-4}$$

$$F_{4-(1+2)} = \frac{A_{(1-2)}}{A_4} F_{(1+2)-4}$$

$$F_{4-2} = F_{4-(1+2)} - F_{4-1}$$

$$F_{2-4} = \frac{A_4}{A_2} F_{4-2}$$

Thus F_{1-4}, F_{2-4}, F_{4-1}, and F_{4-2} are determined. By a similar procedure F_{1-6}, F_{2-6}, F_{6-1}, F_{6-2} are determined. Other internal view factors, such as F_{4-6} are determined by the expression $F_{4-6} = A_6/A_{sphere}$, where A_{sphere} is the total spherical area. This was all done by a separate computer program for reasons of speed and accuracy. Tables IV and V list the internal shape factors.

TABLE IV. - INTERNAL SHAPE FACTORS FOR THE 150° FOOTPRINT CONFIGURATION

[This matrix is referred to as |B|.]

	1	2	3	4	5	6	7	8	9	10	11	12	13	14	15
1	0.00767	0.02256	0.03683	0.04999	0.06163	0.07139	0.07899	0.08419	0.04325	0.04358	0.04358	0.04325	0.04259	0.2394	0.1362
2	.0076	.02254	.03683	.04999	.06163	.07139	.07899	.08419	.04325	.04358	.04358	.04325	.04259	.23506	.13553
3	.0076	↓	↓	↓	↓	↓	↓	↓	↓	↓	↓	↓	↓	.23633	.13426
4	.0076	↓	↓	↓	↓	↓	↓	↓	↓	↓	↓	↓	↓	.23846	.13213
5	.0076	↓	↓	↓	↓	↓	↓	↓	↓	↓	↓	↓	↓	.24178	.12881
6	↓	↓	↓	↓	↓	↓	↓	↓	↓	↓	↓	↓	↓	.24686	.12373
7	↓	↓	↓	↓	↓	↓	↓	↓	↓	↓	↓	↓	↓	.25473	.11586
8	↓	↓	↓	↓	↓	↓	↓	↓	↓	↓	↓	↓	↓	.26719	.10340
9	↓	↓	↓	↓	↓	↓	↓	↓	↓	↓	↓	↓	↓	.28097	.08962
10	↓	↓	↓	↓	↓	↓	↓	↓	↓	↓	↓	↓	↓	.29367	.07692
11	↓	↓	↓	↓	↓	↓	↓	↓	↓	↓	↓	↓	↓	.30990	.06069
12	↓	↓	↓	↓	↓	↓	↓	↓	↓	↓	↓	↓	↓	.33045	.04014
13	.0076	.02254	.03683	.04999	.06163	.07139	.07899	.08419	.04325	.04358	.04358	.04325	.04259	.35599	.01459
14	.01041	.03105	.05098	.06981	.08726	.10322	.11784	.13173	.07116	.07495	.07909	.08369	.08879	0	0
15	.01654	.04891	.07912	.10568	.12702	.14134	.14642	.13928	.06201	.05363	.04232	.02777	.00994	0	0

TABLE V. - INTERNAL SHAPE FACTORS FOR THE 30° FOOTPRINT CONFIGURATION

[This matrix is referred to as |B|.]

	1	3	3	4	5	6	7	8	9	10	11	12
1	0.01705	0.04997	0.07949	0.10359	0.12064	0.12946	0.12946	0.12064	0.10359	0.07949	0.04997	0.01705
2	↓	↓	↓	↓	↓	↓	↓	↓	↓	↓	↓	↓
3	↓	↓	↓	↓	↓	↓	↓	↓	↓	↓	↓	↓
4	↓	↓	↓	↓	↓	↓	↓	↓	↓	↓	↓	↓
5	↓	↓	↓	↓	↓	↓	↓	↓	↓	↓	↓	↓
6	↓	↓	↓	↓	↓	↓	↓	↓	↓	↓	↓	↓
7	↓	↓	↓	↓	↓	↓	↓	↓	↓	↓	↓	↓
8	↓	↓	↓	↓	↓	↓	↓	↓	↓	↓	↓	↓
9	↓	↓	↓	↓	↓	↓	↓	↓	↓	↓	↓	↓
10	↓	↓	↓	↓	↓	↓	↓	↓	↓	↓	↓	↓
11	.01705	.04997	.07949	.10359	.12064	.12946	.12946	.12064	.10359	.07949	.04997	.01705
12	.01732	.05082	.08084	.10535	.12268	.13165	.13165	.12268	.10535	.08084	.05082	0

External shape factors. - The external shape factors were determined using another computer program as well as a graphical analysis. This was done by first finding the view factor of a node to the total lunar surface by using the expression

$$F_{i-M} = 0.5 (1 + \cos \theta)$$

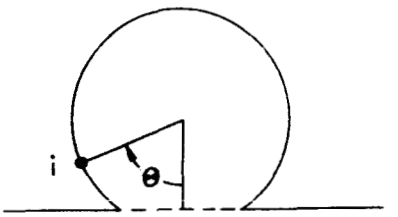

This expression should be integrated over the whole node, but for nodes of less than 15^{o}, using the mid-point of the node to represent the whole node results in no appreciable error.

For node 13 in the 150^{o} footprint configuration, θ is $(75 + 80)/2 = 77.5.^{o}$ This gives a view factor to the lunar surface of $F_{13-M} = 0.6081 = 0.5 (1 + \cos \theta)$. However, the view factors of nodes 16, 17, and 18 are desired. Thus $F_{13-M} = 0.6081 = F_{13-16} + F_{13-17} + F_{13-18}$. A combination computer program and graphical method utilizing the unit hemisphere concept described in reference 4 permits the determination of F_{13-16} and $F_{13-(16 + 17)}$. Thus the shape factors can be determined by:

$$F_{13-17} = F_{13-(16 + 17)} - F_{13-16}$$

$$F_{13-18} = F_{13-M} - F_{13-17} - F_{13-16}.$$

Using area ratios, the reverse shape factors are determined:

$$F_{16-13} = \frac{A_{13}}{A_{16}} F_{13-16}$$

$$F_{17-13} = \frac{A_{13}}{A_{17}} F_{13-17}$$

$$F_{18-13} = \frac{A_{13}}{A_{18}} F_{13-18} \approx 0.$$

In this manner, all the external shape factors can be determined. The shape factors for the 150^{o} footprint configuration are listed in table VI and those for the 30^{o} footprint are listed in table VII.

TABLE VI. - EXTERNAL SHAPE FACTORS FOR THE 150° FOOTPRINT CONFIGURATION

[This matrix is referred to as |C| .]

	1	2	3	4	5	6	7	8	9	10	11	12	13	16	17	18
1	0	0	0	0	0	0	0	0	0	0	0	0	0	0	0	0.0019
2	0	0	0	0	0	0	0	0	0	0	0	0	0	0	0	.0170
3	0	0	0	0	0	0	0	0	0	0	0	0	0	0	0	.0485
4	0	0	0	0	0	0	0	0	0	0	0	0	0	0	0	.0904
5	0	0	0	0	0	0	0	0	0	0	0	0	0	0	0	.1464
6	0	0	0	0	0	0	0	0	0	0	0	0	0	0	0.0174	.1958
7	0	0	0	0	0	0	0	0	0	0	0	0	0	0.0095	.0524	.2268
8	0	0	0	0	0	0	0	0	0	0	0	0	0	.0473	.0947	.2286
9	0	0	0	0	0	0	0	0	0	0	0	0	0	.1148	.1712	.1987
10	0	0	0	0	0	0	0	0	0	0	0	0	0	.189	.123	.1664
11	0	0	0	0	0	0	0	0	0	0	0	0	0	.287	.111	.1238
12	0	0	0	0	0	0	0	0	0	0	0	0	0	.421	.070	.0742
13	0	0	0	0	0	0	0	0	0	0	0	0	0	.556	.026	.0261
16	0	0	0	0	0	0	0.0025	0.0131	0.0163	0.0271	0.0411	0.0599	0.0778	0	0	0
17	0	0	0	0	0	0.0029	.0097	.0186	.0123	.0125	.0113	.0071	.0026	0	0	0

TABLE VII. - EXTERNAL SHAPE FACTORS FOR THE 30° FOOTPRINT CONFIGURATION

[This matrix is referred to as |C| .]

	1	2	3	4	5	6	7	8	9	10	11	13	14	15	16	17
1	0	0	0	0	0	0	0	0	0	0	0	0	0	0	0	0.0047
2	0	0	0	0	0	0	0	0	0	0	0	0	0	0	0	.04
3	0	0	0	0	0	0	0	0	0	0	0	0	0	0	0	.103
4	0	0	0	0	0	0	0	0	0	0	0	0	0	0	0	.195
5	0	0	0	0	0	0	0	0	0	0	0	0	0	0	0.017	.291
6	0	0	0	0	0	0	0	0	0	0	0	0	0	0.0141	.507	.37
7	0	0	0	0	0	0	0	0	0	0	0	0	0.0022	.0778	.116	.367
8	0	0	0	0	0	0	0	0	0	0	0	0	.0441	.2155	.1504	.2811
9	0	0	0	0	0	0	0	0	0	0	0	0.0129	.2511	.246	.115	.1791
10	0	0	0	0	0	0	0	0	0	0	0	.379	.335	.106	.029	.047
11	0	0	0	0	0	0	0	0	0	0	0	.92893	.01894	.00665	.00239	.0046
13	0	0	0	0	0	0	0	0	0.0142	0.3186	0.4920	0	0	0	0	0
14	0	0	0	0	0	0	0.00205	0.0384	.1872	.1918	.0068	0	0	0	0	0
15	0	0	0	0	0	0.00585	.0323	.0833	.0815	.0269	.0011	0	0	0	0	0
16	0	0	0	0	0.0047	.0150	.0343	.0415	.0272	.0053	.0003	0	0	0	0	0

Direct Solar and/or Albedo Heating

The real nodes receive heating from direct solar (solar spectrum) heating or from solar radiation reflected from the moon's surface. Letting A stand for area, the direct solar heating is simply:

for nodes on balloon: $S \cdot \alpha_B \cdot A_{normal}/A_{node}$;

for nodes on moon: $S \cdot \alpha_M \cdot 1$.

For the moon, the normal area of a node is the same as the area of the node. Obviously, on the balloon only the nodes that have an outward normal component in the direction of the sun will have a direct solar heating term.

Nodes on the balloon will also have an albedo heating contribution. This is merely:

$$S(1 - \alpha_M) F_{i-M} \alpha_B ,$$

where F_{i-M} is the shape factor of node "i" to the total lunar surface. Thus the total heating term (Q_i) on node i will be:

$$Q_i = S \cdot \alpha_B \left[\frac{A_{normal\ i}}{A_{node\ i}} + F_{i-M} (1 - \alpha_M) \right]$$

These Q_i's will pertain only to real nodes. In the matrices (tables IV through VII) these Q_i terms are in the extreme right column.

RESULTS

The results have been both tabulated and graphically presented to best show any trends in temperatures. Data is presented in tabulated form in table VIII. Figure 2 shows a sketch of the node locations for the 150° and 30° footprint cases. A polar plot of the temperature profiles for the first eight cases (the 150° footprint) is shown in figure 4, and the profiles for cases 9 and 10 (the 30° footprint) are shown in figure 5. These two plots show that the temperature at the top of the sphere starts either above or below the lunar surface temperature depending on the coating. Going down the side of the sphere (toward the equator), the temperatures approach the lunar surface temperature. This is the only trend shown for the 150° footprint configuration, since there is very little shadowing. The 30° footprint configuration shows this trend going slightly below the equator, and then the temperatures decrease going down into the shadowed crevice made by the balloon and the lunar surfaces. Linear plots of balloon temperatures are shown in figures 6 and 7.

The temperatures of the flat spots or base of the balloon are very close to the arithmetic average of all the balloon temperatures. Figure 8 is a plot of these average temperatures versus ϵ_{BO} for varying α_B's. Figure 9 is a plot of average temperatures versus α_B for various ϵ_{BO}'s. The points for the 30° footprint were also plotted on these two curves, showing a steeper line in figure 8 and a convergence in figure 9. This convergence implies that as the balloon becomes more spherical, the hotter coating temperatures decrease and the cooler temperatures increase.

A coating having the highest emittance, $\epsilon_{BO} = 0.4$, and the most data points, $\alpha_B = 0.15$, was used as the standard for evaluating lunar emittance effects for the 150° footprint in figure 10. The range considered is broad enough to encompass the maximum lunar temperatures that appear in the literature. The balloon temperatures change only 5 to 10°F, and thus are not strongly affected by lunar temperatures.

TABLE VIII. - TEMPERATURES FOR THE CASES EVALUATED

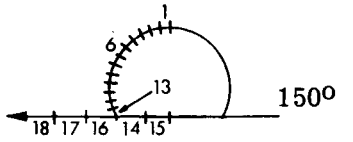

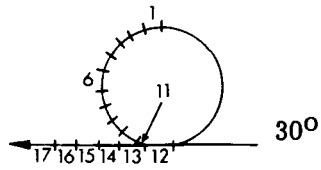

Property	Case number									
	1	2	3	4	5	6	7	8	9	10
Balloon absorptance	0.10	0.15	0.20	0.10	0.15	0.20	0.15	0.15	0.15	0.15
Balloon external emittance	.03	.03	.03	.40	.40	.40	.15	.28	.03	.40
Balloon internal emittance	.40	.40	.40	.40	.40	.40	.40	.40	.40	.40
Lunar absorptance	.93	.93	.93	.93	.93	.93	.93	.93	.93	.93
Lunar emittance	.85	.85	.85	.85	.85	.85	.85	.85	.85	.85
Footprint angle,degree	150	150	150	150	150	150	150	150	30	30
Node temperatures, °F										
1	368	443	503	84	116	144	216	151	388	121
2	367	442	502	86	117	144	215	151	386	124
3	366	441	500	90	119	145	214	152	382	127
4	364	438	498	95	122	145	212	152	376	133
5	362	435	494	101	125	146	209	153	369	139
6	359	432	490	108	129	147	206	153	360	145
7	356	428	486	115	132	148	202	153	357	158
8	352	423	481	122	136	149	197	153	358	170
9	349	420	477	127	139	149	194	153	357	162
10	347	417	474	131	141	150	191	153	354	124
11	346	416	473	137	145	153	192	155	353	111
12	347	417	473	144	152	160	195	161	365	144
13	347	417	473	151	159	169	198	166	80	73
14	355	427	485	119	135	150	202	154	39	29
15	356	428	486	115	133	149	203	154	291	289
16	290	290	291	287	288	288	289	288	280	279
17	273	273	273	272	273	273	273	273	267	267
18	267	267	267	267	267	267	267	267		

Figures 11 and 12, linear plots for the temperatures of all 10 cases, are similar to figures 6 and 7 except that a lunar emittance, ϵ_M, of 0.91 instead of 0.85 is used. This is considered to be more in agreement with lower lunar temperatures of 254°F. These graphs reflect the same results as figure 10; the temperatures change very little. In fact, figures 11 and 12 as plotted are almost identical to figures 6 and 7. This further shows the relative insensitivity of the balloon temperatures to the moon's temperatures.

CONCLUSIONS

Any temperature limitations of the plastic skin can be alleviated by increasing the total emittance of the external surface. For example, if the film were one-fourth mil Mylar with about 500 angstroms of aluminum and had an upper temperature limit of 250°F, an α_B/ϵ_{BO} (solar absorptance/total emittance) of one or less would be adequate. This could be achieved with a couple of microns of a quartz type (silicon monoxide) coating over the aluminized Mylar. There does not seem to be any great problem in maintaining proper thermal control, provided the termal coating does not degrade excessively throughout the lifetime of the balloon.

Degradation of thermal coatings appears to be a significant factor in this application. This degradation is caused primarily by the combination of vacuum, ultraviolet radiation, and the corpuscular radiation of the solar wind (the latter is significant, since the moon has no magnetic field for shielding protection as does the earth). The silicon monoxide on aluminized Mylar described above may resist degradation as well or better than white paints, and has a large weight advantage.

This analysis has proved the thermal feasibility of the lunar balloon, provided that degradation of the thermal coating is not excessive.

RECOMMENDATIONS

Further areas for development of the thermal design of the lunar balloon involve test and analytical studies as well as coating selection.

Testing of thermal coatings would involve evaluation of solar absorptance and emittance, flexibility and adhesion, and degradation under the lunar environment. Figures 13 and 14 show test data for aluminized Mylar with a SiO dielectric. Reference 5 reports an alternate dielectric that may be considered. White paints or dyed films represent another coating possibility. The former may be applied in thin layers of 0.5 to 5 mils, with the thinner layers being slightly transparent but with a high reflectance.

The thermal analysis of this report could be extended if desired to evaluate other coatings, either opaque or transparent. Evaluation of transparent coatings would require modification of the analytical thermal model.

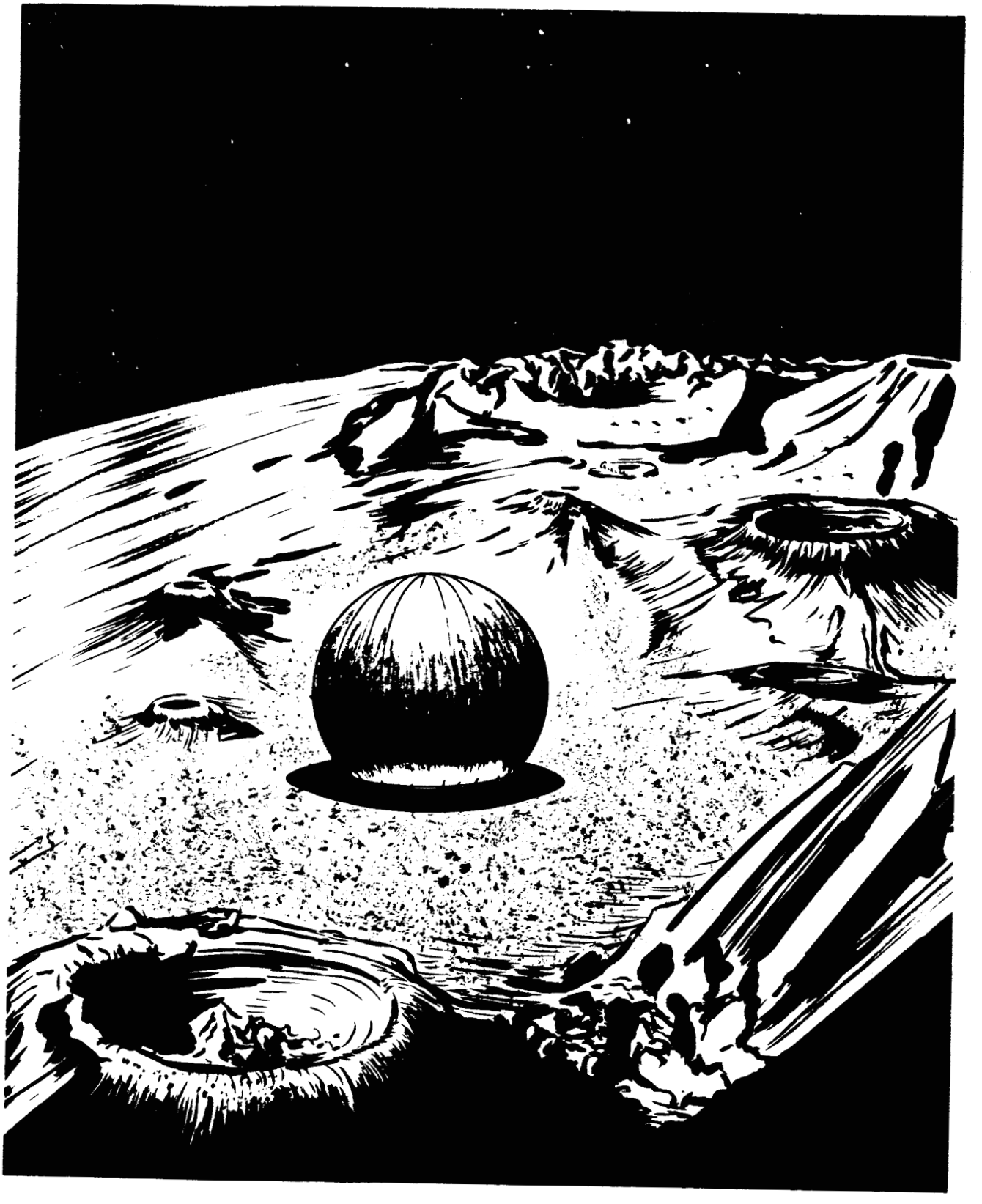

Figure 1. - Sphere on Moon.

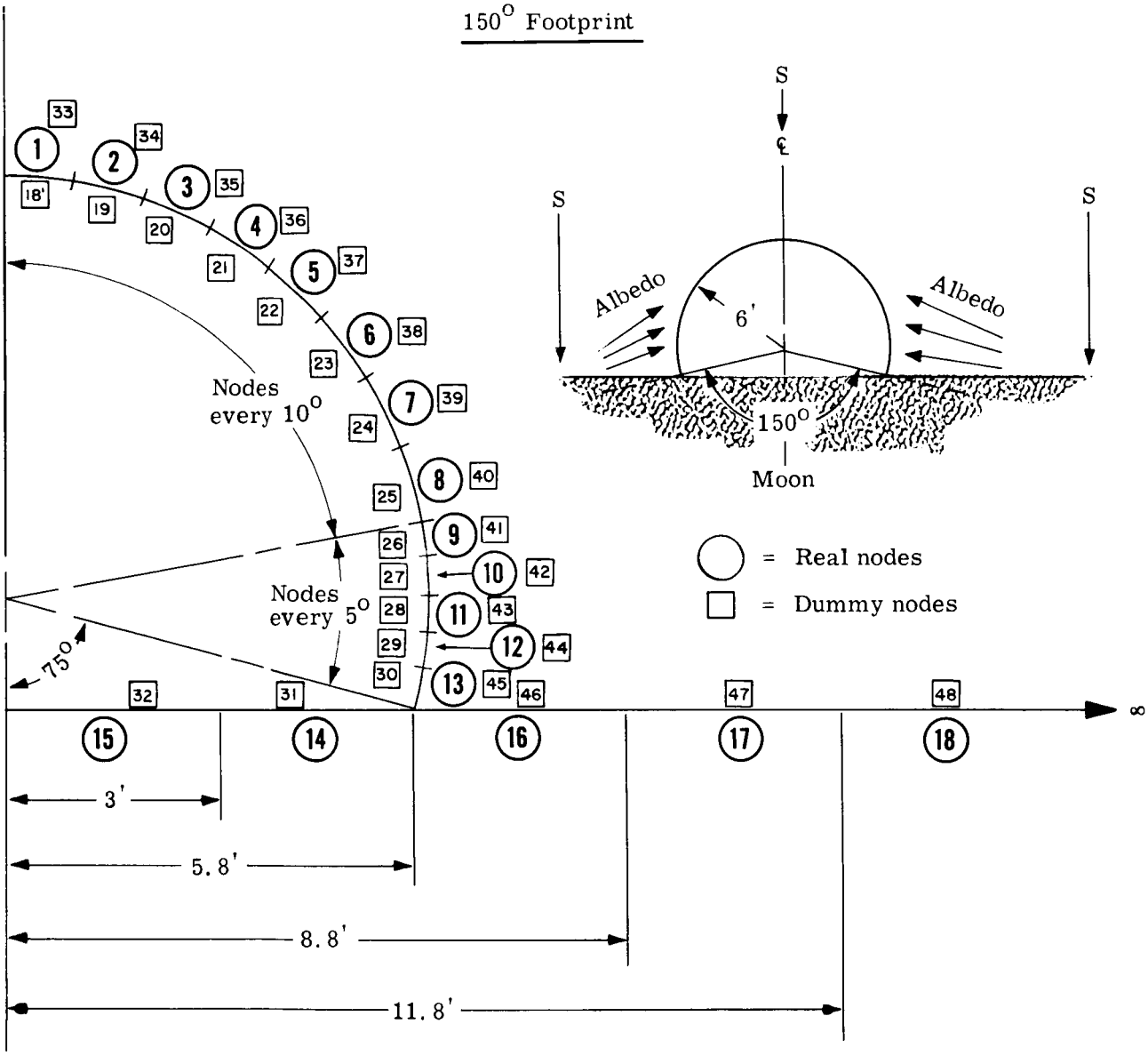

Figure 2. - Thermal schematic of balloon - node locations.

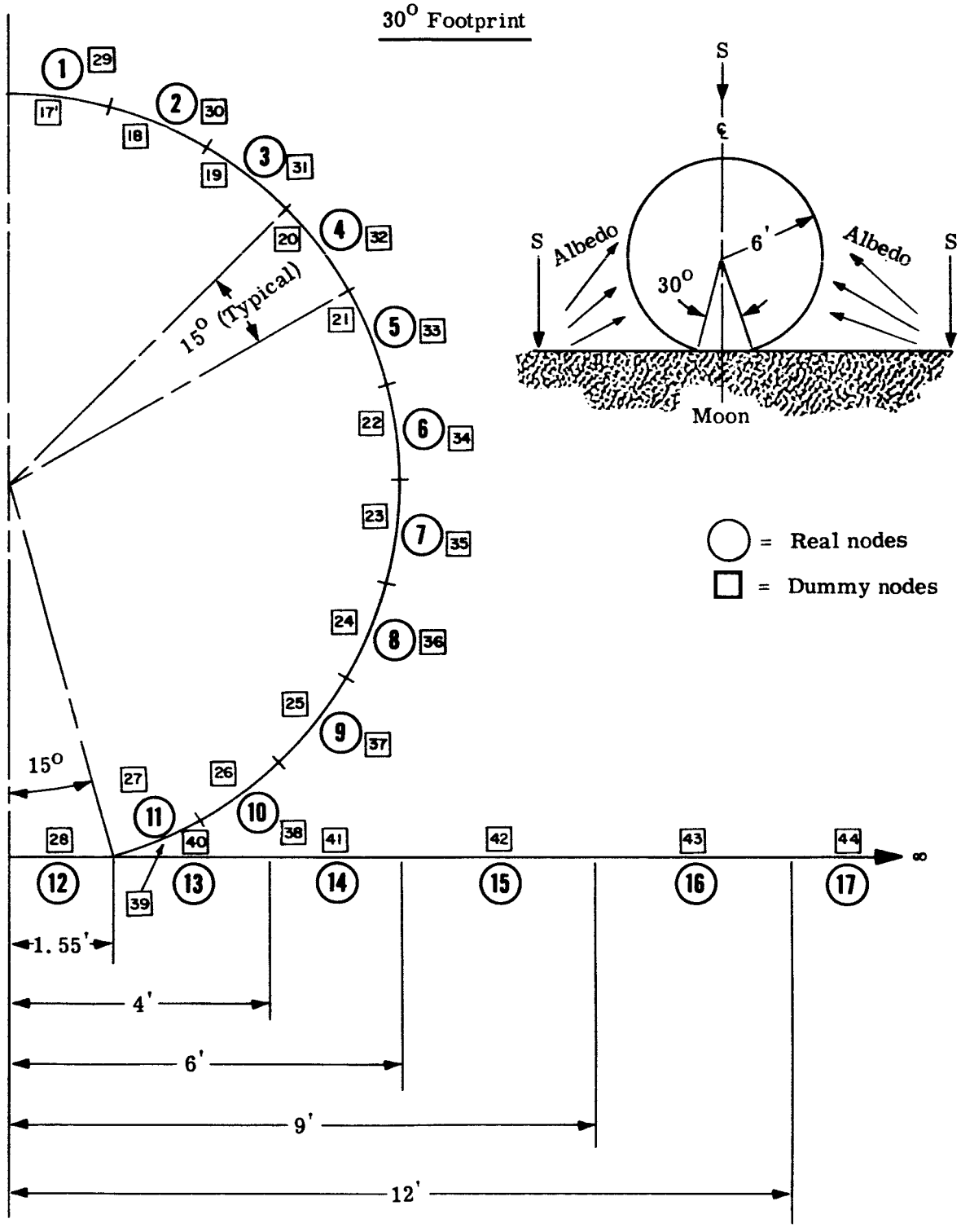

Figure 2. - Concluded.

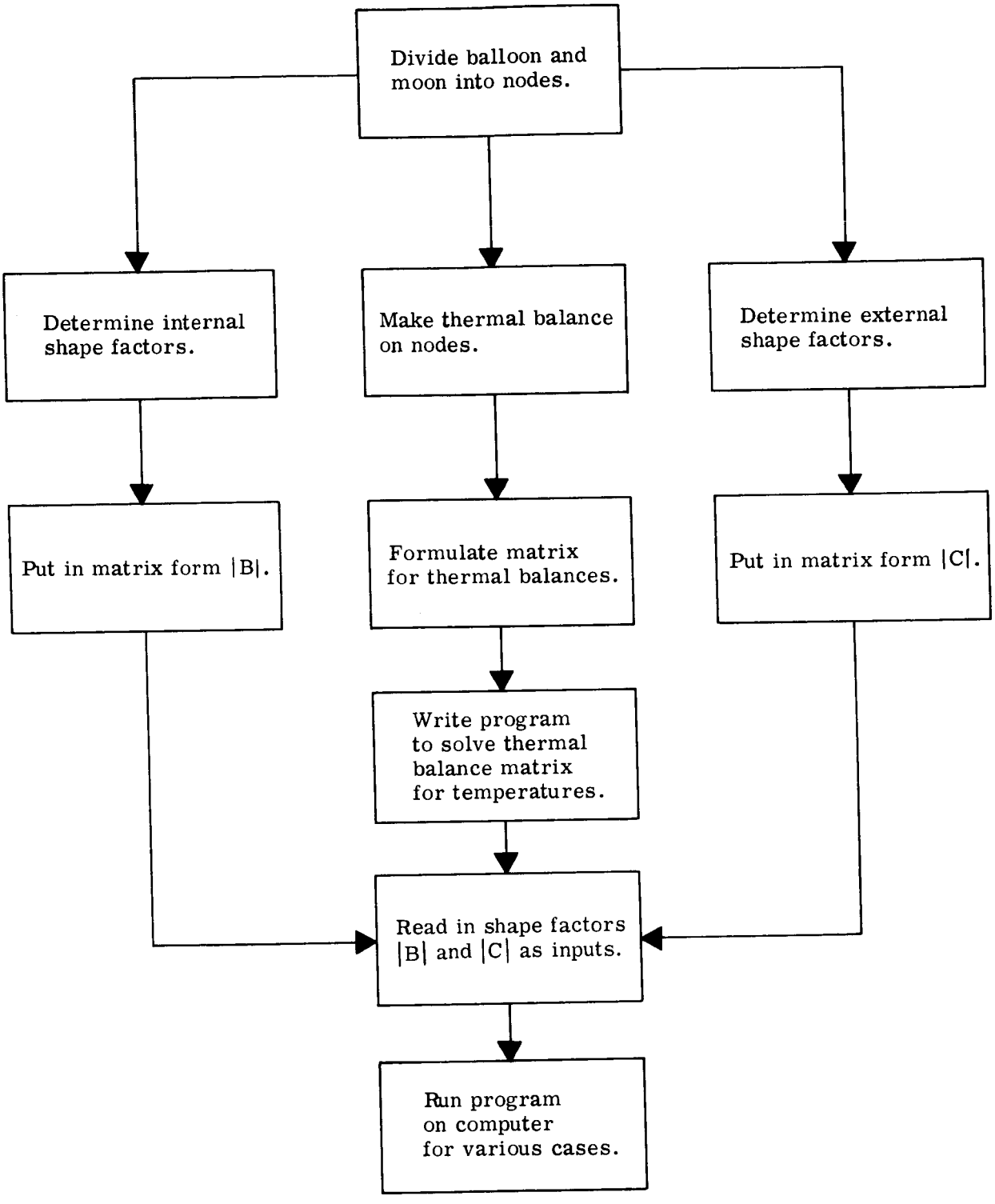

Figure 3. - Flow chart of analytical procedure.

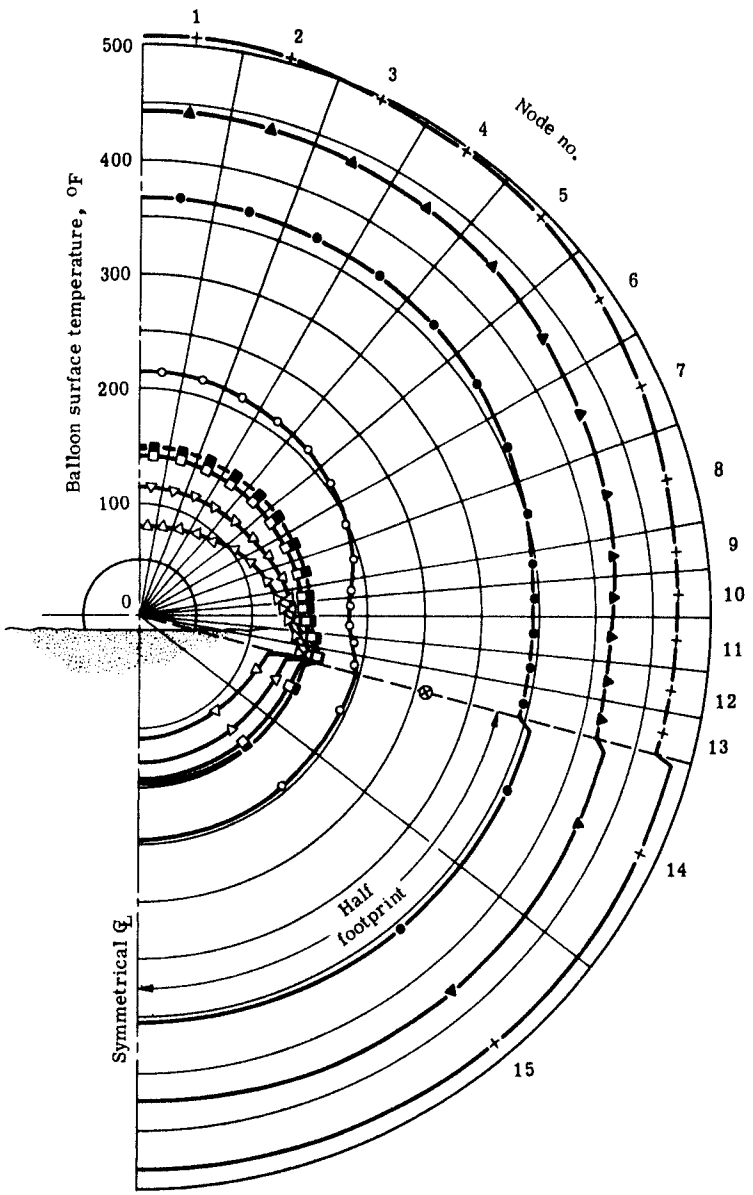

Symbol	Case no.	α_B	ϵ_{BO}	α_B/ϵ_{BO}	T_{avg}, °F	T_{max}, °F	T_{min}, °F
●	1	0.10	0.03	3.330	355	368	346
▲	2	0.15	0.03	5.000	427	443	416
+	3	0.20	0.03	6.700	485	503	473
△	4	0.10	0.40	0.250	117	151	84
▽	5	0.15	0.40	0.375	134	159	116
□	6	0.20	0.40	0.500	149	169	144
○	7	0.15	0.15	1.000	202	216	191
■	8	0.15	0.28	0.536	154	166	151

$\epsilon_I = 0.4$

$\alpha_{moon} = 0.93$

$\epsilon_{moon} = 0.85$

Footprint = 150°

⊗ Moon temperature, °F	289	273	267
Distance from balloon edge, ft	0 - 3	3 - 6	6 - ∞

Figure 4. - Polar plot of temperatures for the 150° footprint configuration.

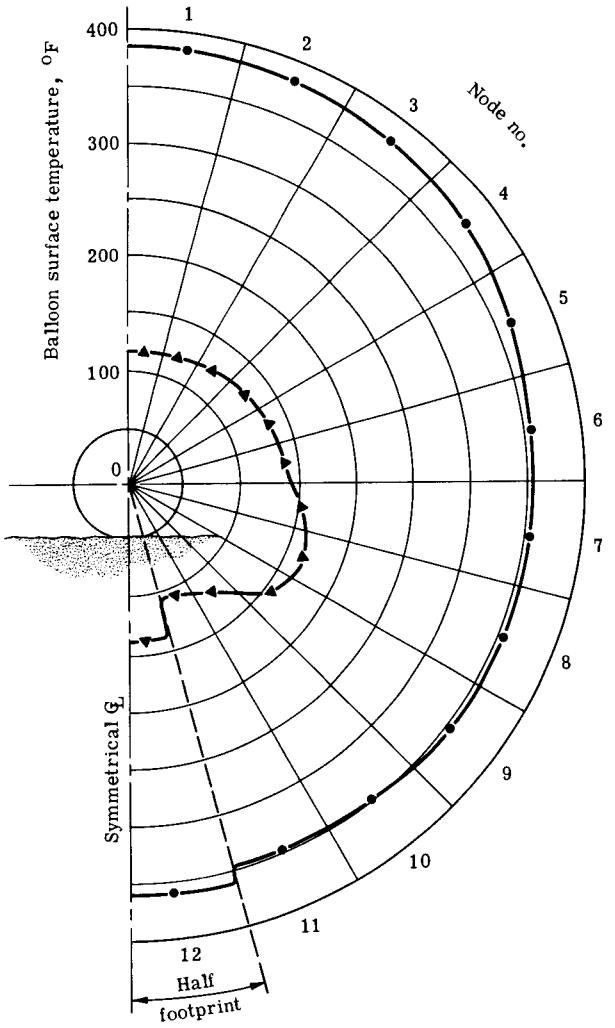

Symbol	Case no.	α_B	ϵ_{BO}	α_B/ϵ_{BO}	$T_{avg.}$ °F	$T_{max.}$ °F	$T_{min.}$ °F
●	9	0.15	0.03	5.0	365	388	353
▲	10	0.15	0.40	0.375	144	170	111

$\epsilon_I = 0.4$

$\alpha_{moon} = 0.93$

$\epsilon_{moon} = 0.85$

Footprint = 30°

Figure 5. - Polar plot of temperatures for the 30° footprint configuration.

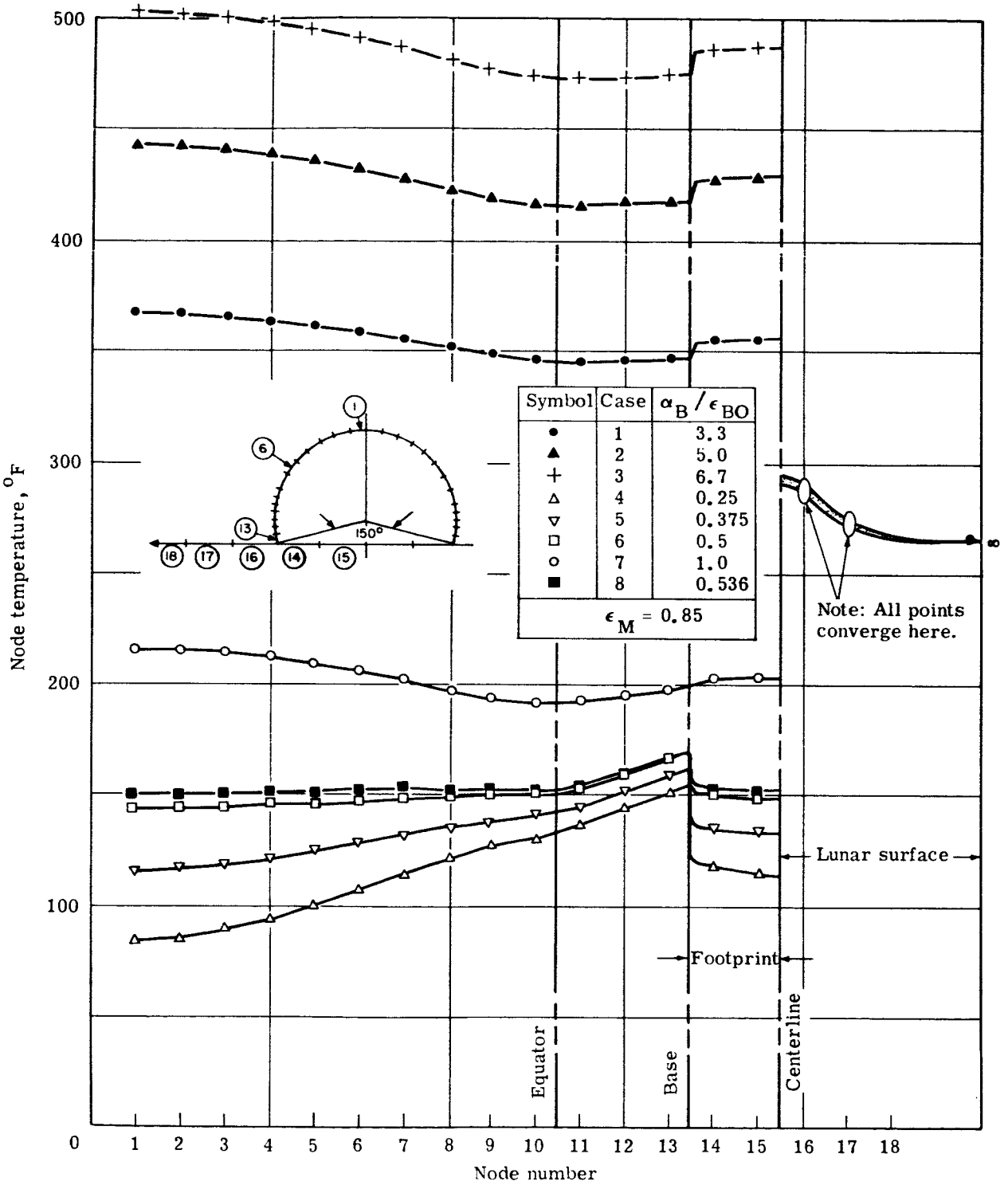

Figure 6. - Linear plot of temperatures for the 150° footprint configuration.

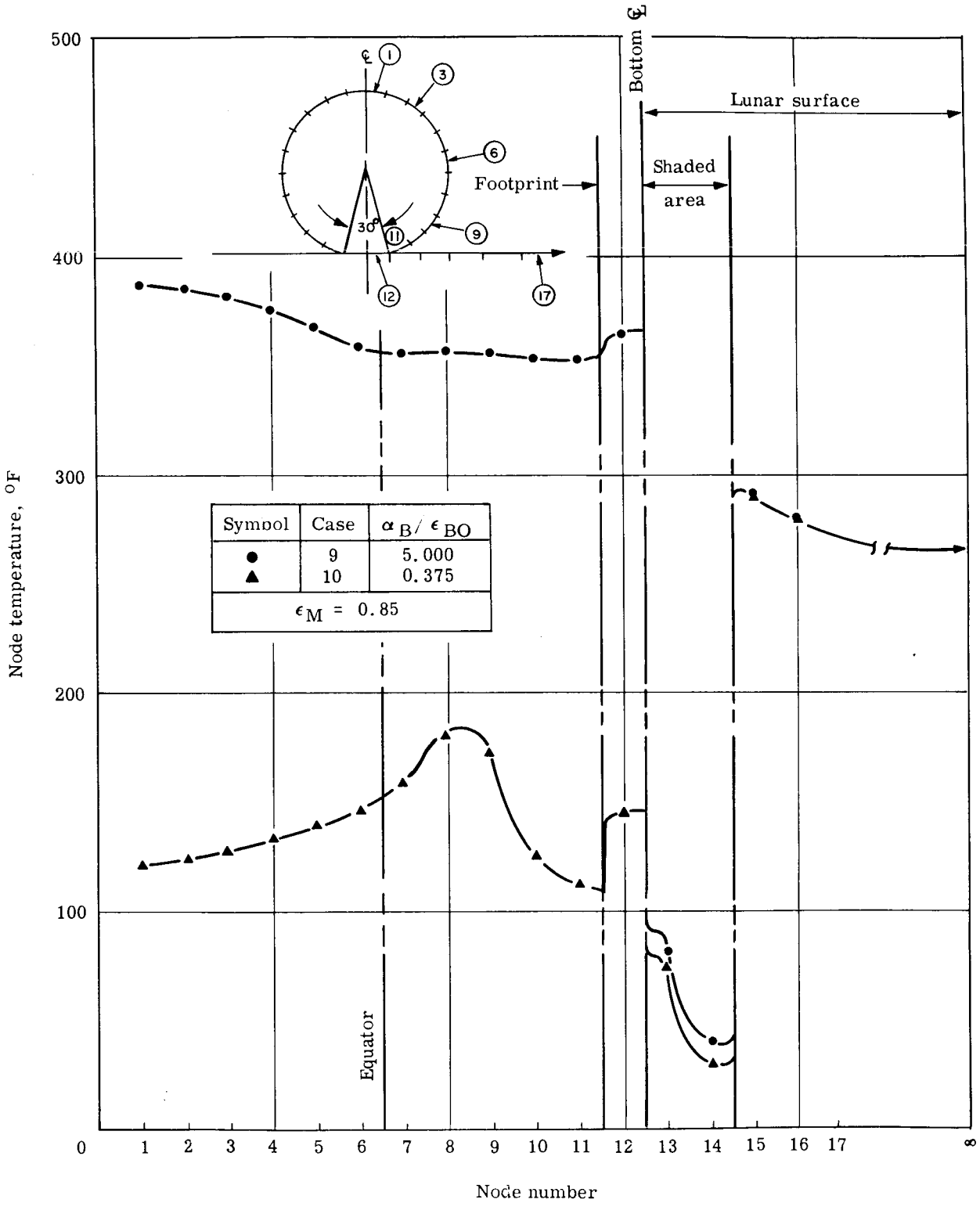

Figure 7. - Linear plot of temperatures for the 30° footprint configuration.

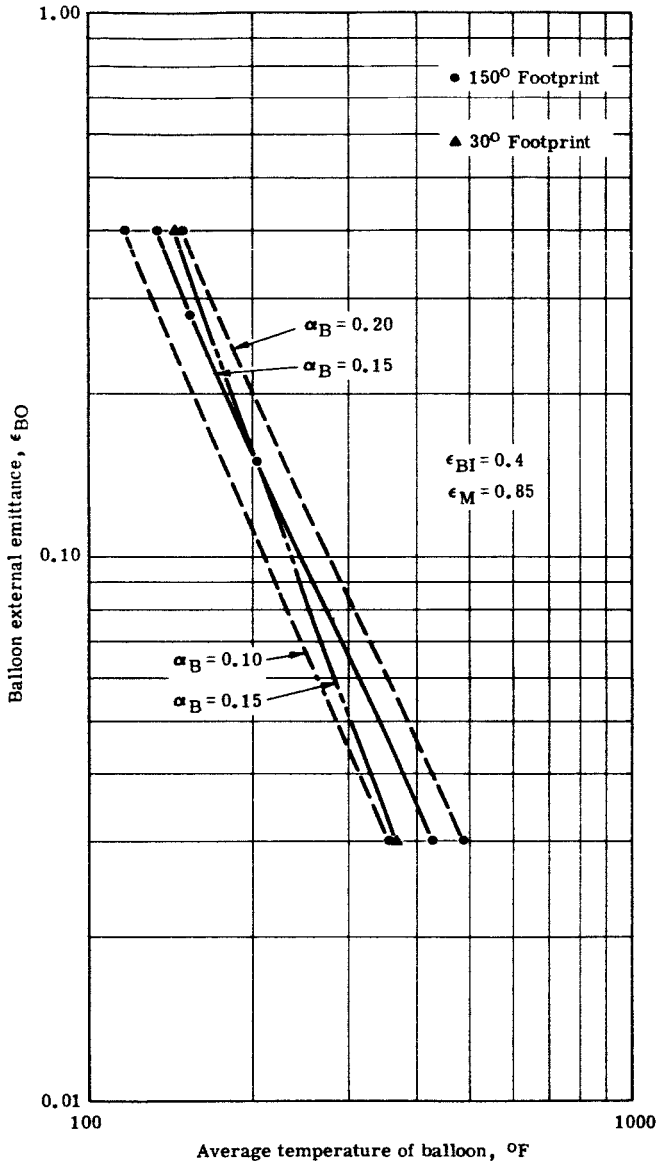

Figure 8. - Effect of balloon emittance on average balloon temperatures.

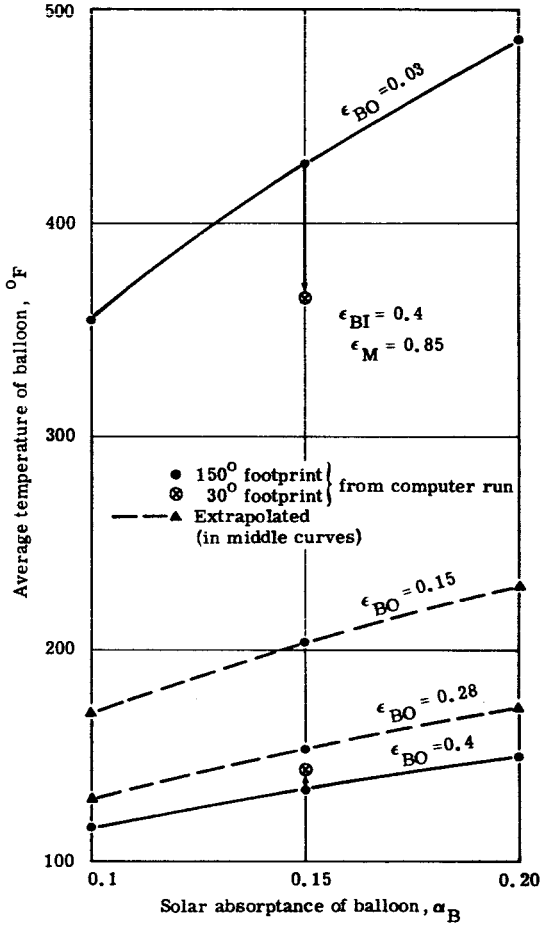

Figure 9. - Effect of balloon absorptance on average balloon temperatures.

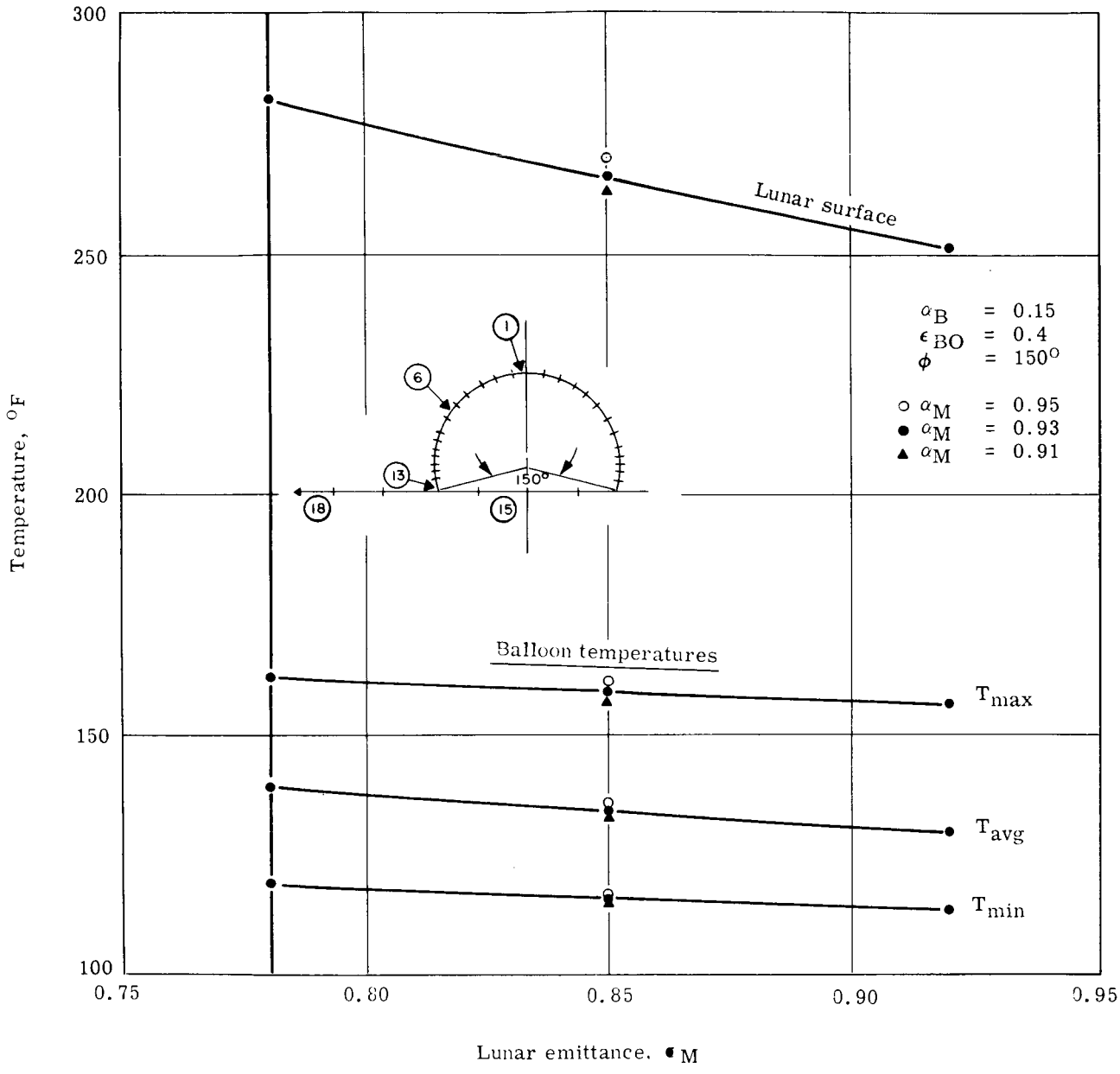

Figure 10. - Effect of lunar surface properties on average balloon temperatures.

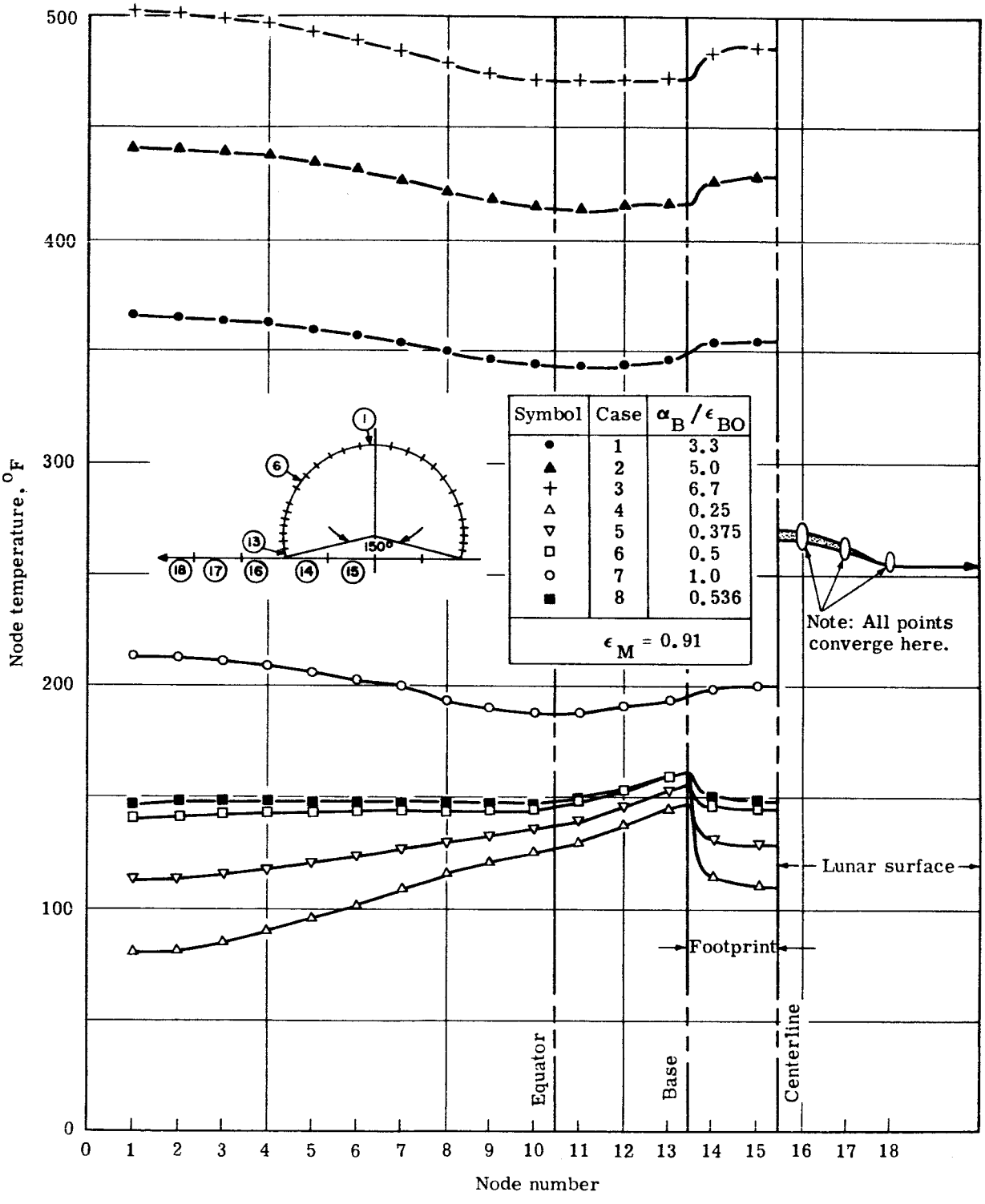

Figure 11. - Linear plot of temperature for 150° footprint, $\epsilon_M = 0.91$.

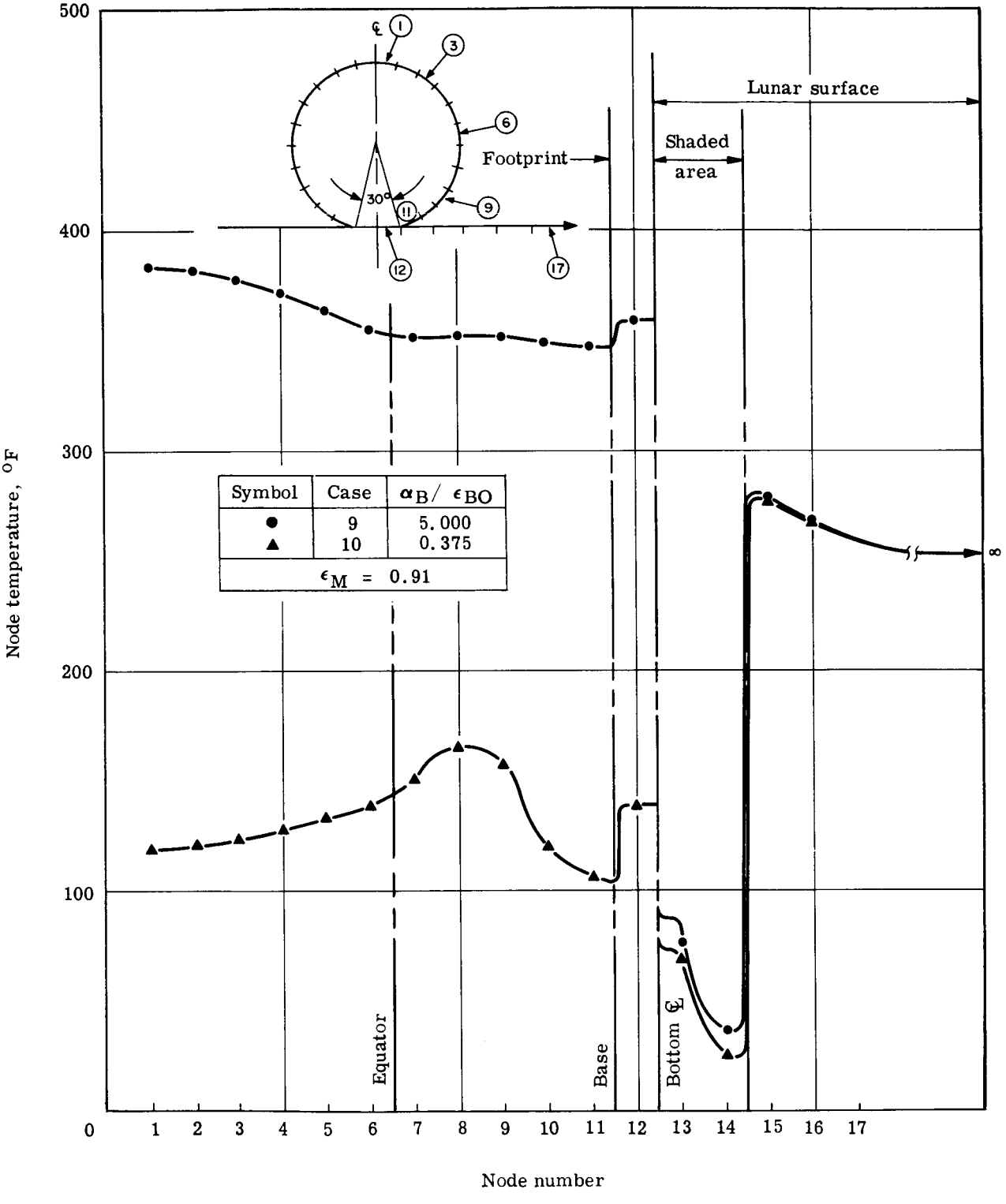

Figure 12. - Linear plot of temperature for 30^{o} footprint, ϵ_M = 0.91.

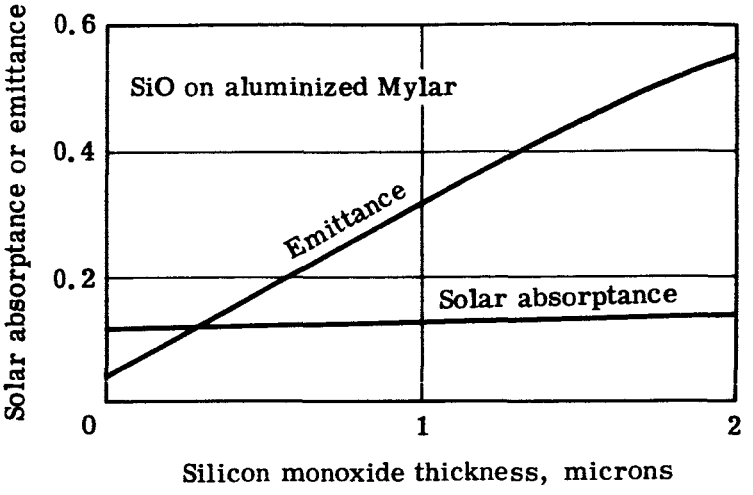

Figure 13. - Radiation properties of dielectrics.

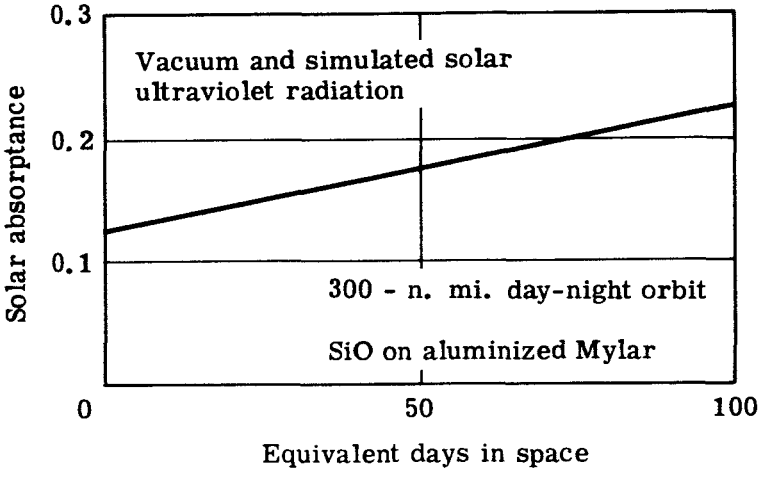

Figure 14. - Dielectric degradation in space.

REFERENCES

1. Gold, Thomas: Recent Evidence Concerning the Lunar Surface. Advances in the Astronautical Sciences, vol. 18, 1964, p. 44.

2. Oppenheim, A. K.: in Trans. ASME, vol. 78, 1956, pp. 725+.

3. Geoffrion, Ann R., et al: Isothermal Contours of the Moon. Lowell Observatory Bulletin No. 106, vol. 5, May 27, 1960.

4. Eckert, E. R. G.; and Drake, R. M.; Jr.: Heat and Mass Transfer. McGraw-Hill Book Co., Inc., 1959.

5. Hass, G., et al: Solar Absorptance and Thermal Emittance of Aluminum Coated with Surface Films of Evaporated Aluminum Oxide. AIAA 65-656, September, 1965.